

Linear and non-linear optical properties of AgBO_3 (B=Nb, Ta): first principle study

Sevket Simsek

Nanotechnology Research Center (NANOTAM)
Bilkent University
06800, Ankara, Turkey
sevkets@bilkent.edu.tr

Amirullah M.Mamedov, Ekmel Ozbay

Nanotechnology Research Center (NANOTAM)
Bilkent University
06800, Ankara, Turkey
mamedov@bilkent.edu.tr, ozbay@bilkent.edu.tr

Abstract—The linear and nonlinear optical properties of ferroelectrics AgBO_3 (B=Ta, Nb) are studied by density functional theory (DFT) in the local density approximation (LDA) expressions based on first principle calculations without the scissor approximation. Specially, we present calculations of the frequency-dependent complex dielectric function $\epsilon(\omega)$, and the second harmonic generation response coefficient $\chi^{(2)}(-2\omega, \omega, \omega)$ over a large frequency range in rhombohedral phase for the first time. The electronic linear electrooptic susceptibility $\chi^{(2)}(-\omega, \omega, 0)$ is also evaluated below the band gap. These results are based on a series of the LDA calculation using DFT.

Keywords—ferroelectric; nonlinear optics; AgTaO_3 ; AgNbO_3

I. INTRODUCTION

Nowadays, nonlinear optics has developed a field of major study because of rapid advance in photonics [1]. Nonlinear optical techniques have been applied to many diverse disciplines such as condensed matter physics, medicine and chemical dynamics. The development of new advanced nonlinear optical materials for special applications is a crucial importance in technical areas such as optical signal processing and computing, acousto-optic devices and artificial neuro-network implementation. There are intense efforts in experimenting, fabricating and searching for various nonlinear optical materials including ferroelectrics and related compounds. However there is comparatively a much smaller effort to understand the nonlinear optical processes in these materials at the microscopic level. Theoretical understanding of the factor that control the figure of merit is extremely important in improving the existing electrooptic (EO) materials and in the search for new ones [2].

In this paper, we describe details calculations of the linear and nonlinear optical properties, includes linear electro-optic tensor for AgBO_3 ferroelectrics with oxygen octahedral structure.

II. COMPUTATIONAL DETAILS

The nonlinear optical properties of AgBO_3 were theoretically studied by means of first principles calculations in the framework of density functional theory (DFT) and based on the local density approximation (LDA) [6] as implemented in

the ABINIT code [3,7]. The self-consistent norm-conserving pseudopotentials are generated using Troullier-Martins scheme [8] which is included in the Perdew-Wang [9] scheme as parameterized by Ceperly and Alder [10]. For calculations, the wave functions were expanded in plane waves up to a kinetic-energy cutoff of 42 Ha for rhombohedral AgTaO_3 and 70 Ha for orthorhombic AgNbO_3 . Pseudopotentials are generated using the following electronic configurations: For Ag[Kr], the $4d^{10}5s^1$ electron is considered as the true valence. For Nb[Kr], $4d^4 5s^1$, and for Ta[Xe], $6s^2 5d^3$, electron states are treated as valence states. For O, only the true valence states ($2s^2$ and $2p^4$) are taken into account. The Brillouin zone for both compounds was sampled using a $8 \times 8 \times 8$ the Monkhorst-Pack [11] mesh of special k points.

III. RESULTS

A. Electronic Band Structure and Density of State (DOS)

AgBO_3 (B=Nb, Ta) has a $R3c$ and $Pmc2_1$ symmetries, respectively. The unit cell for AgTaO_3 contains two formula units with 10 atoms and the unit cell for AgNbO_3 contains eight formula units with 40 atoms. The calculated electronic band structures and total DOS are shown in Fig. 1 and Fig. 2. For AgTaO_3 the lowest point of the conduction band is at the D high symmetry point of the BZ, and the highest point of the valence band is at the X high symmetry point of the BZ. It is an indirect band gap material. AgNbO_3 is isostructural material and its band dispersion behave very similarly (Fig. 1) to AgTaO_3 . For AgNbO_3 the lowest point of the conduction band is at the S point of the BZ, and the highest point of the valence band is at the T point of the BZ. The calculated indirect band gaps of AgNbO_3 and AgTaO_3 are 1.51 eV and 1.79 eV, respectively. These values smaller than the experimental values ($\Delta E = E_{ge} - E_{gt} = 1.29$ eV and 1.64 eV for the AgNbO_3 and AgTaO_3 , respectively) [12]. This is not surprising, because it is well known that the band gap calculated by DFT is smaller than that obtained from experiments. This error is due to the discontinuity of exchange-correlation energy [3]. For AgTaO_3 and AgNbO_3 , the highest valence band region, ranging from -6 eV to 0 eV, are composed of mainly O 2p states. Also O 2p is hybridized with Ag 4d and somewhat with B nd orbitalals (n=4 and 5 for Nb and Ta, respectively). The bottom-most valence band region, ranging from -18 eV to -16 eV is composed of O 2s and Ta 5s states. The lowest conduction band can be divided

into two regions and originates mainly from the contribution of the localized Nb 4d and Ta 5d –states.

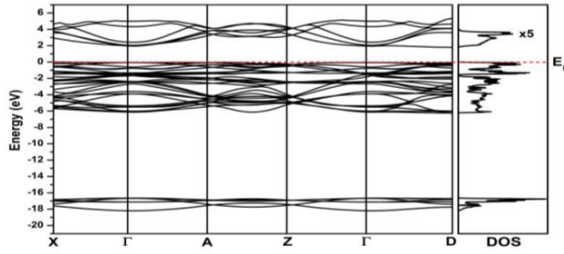


Fig. 1. The calculated electronic band structure of AgTaO₃.

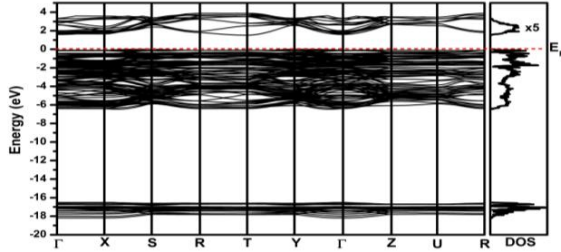


Fig. 2. The calculated electronic band structure of AgNbO₃.

B. Electro-Optic Tensor

In the noncentrosymmetric phases of AgTaO₃ the EO tensor has four independent elements $r_{13} = r_{23}$, r_{33} , $r_{22} = r_{12} = r_{61}$, $r_{51} = r_{42}$. Similarly, the EO of AgNbO₃ has five independent elements r_{13} , r_{23} , r_{33} , r_{42} , and r_{51} . In contrast to the dielectric tensor, the EO coefficients can either be positive or negative. The sign of these coefficients is often difficult to measure experimentally. Moreover, it depends on the choice of the Cartesian axes. The z axis is along the direction of the spontaneous polarization and the y – axis lies in a mirror plane. The z and y –axes are both piezoelectric. Their positive ends are chosen in the direction that becomes negative under compression. The orientation of these axes can easily be found from pure geometrical arguments. Our results are reported in the Cartesian axes where the piezoelectric coefficients d_{22} and d_{33} are positive. These coefficients, as well as their total and electronic part, are reported in Table 1. All EO coefficients are positive as is the case for the noncentro-symmetric phases [3], the phonon modes that have the strongest overlap with the soft mode of the paraelectric phase dominate the amplitude to the EO coefficients. Moreover, the electronic contributions are found to be quite small. EO coefficients matrices for the AgTaO₃ (point group 3m) and AgNbO₃ (point group mm2) are listed below:

Table 1. EO tensors and non-linear optic coefficients of AgTaO₃ crystal.

Crystals	Symmetry Class	EO coefficients (pm/V)		Non-linear optic coefficients (pm/V)		
		Electronic	Total	$d_{31}=d_{15}$	d_{33}	
AgTaO ₃	3c	r_{13}	0.0385	0.3862	$d_{31}=d_{15}$	-0.4368
		r_{33}	0.1042	0.6561	d_{33}	1.128
		$r_{51} = r_{42}$	0.0394	0.2758		

C. Linear Optical Properties

Real and imaginary parts of the dielectric function $\epsilon(\omega) = \epsilon_1(\omega) - i\epsilon_2(\omega)$ as a function of the photon energy for AgTaO₃ and AgNbO₃ along the x- and z-crystallographic axes were calculated and are given in Fig. 3 and Fig. 4.

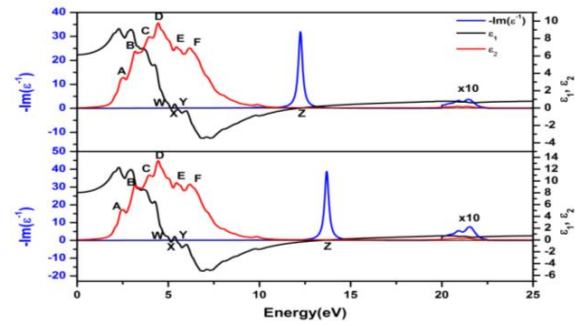


Fig. 3. The calculated real and imaginary of linear dielectric tensor and energy loss function of AgTaO₃ in x-direction (a) and z-direction (b).

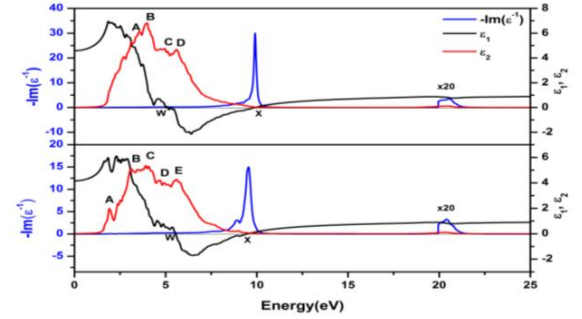


Fig. 4. The calculated real and imaginary of linear dielectric tensor and energy loss function of AgNbO₃ in x-direction (a) and z-direction (b).

As shown in Fig. 3, the peak values of the dielectric function $\epsilon(\omega) = \epsilon_1(\omega) - i\epsilon_2(\omega)$ along the x- and z-crystallographic axes are almost identical. For this reason, we consider only the x- crystallographic direction's results. $\epsilon_1(\omega)$ is equal to zero at W (5.07 eV), X (5.24 eV), Y (5.45 eV) and Z (13.69 eV) for AgTaO₃. For AgNbO₃, $\epsilon_1(\omega)$ is equal to zero at W (5.09 eV) and X (9.86 eV). The peaks of the $\epsilon_2(\omega)$ correspond to the optical transitions from the valence band to conduction band. The function $\epsilon_2(\omega)$ for AgTaO₃ shows peaks at A (2.48 eV), B (3.11 eV), C (3.92 eV), D (4.46 eV), E (5.45 eV) and F (6.18 eV). Whereas the function $\epsilon_2(\omega)$ for AgNbO₃ shows peaks at A (3.55 eV), B (4.00 eV), C (4.493 eV), D (5.626 eV). The calculated energy loss functions along x- and z-axes, $-\text{Im}(1/\epsilon)$, is given in Fig. 3 and Fig. 4. The function $-\text{Im}(1/\epsilon)$ describes the energy loss of fast electrons traversing the material. Generally, the maxima in the energy-loss function are associated with the interband transitions and with the energies of the plasma resonances. The $-\text{Im}(1/\epsilon)$ has a maximum near 13.6 eV, 12.3 eV and structure near 21.0 eV for AgTaO₃, 9.85 eV, 9.50 eV and structure near 22.0 eV for AgNbO₃ along x- and z- axes, respectively. Also, in the energy region above 12 eV there is a drop in $\epsilon_2(\omega)$, there is no sharp structure in its spectrum, which corresponds to exhaustion of the sum rule and the excitation of the plasma vibrations in the valence band.

D. Nonlinear Optical Properties

The fact that the SHG coefficients are related to the optical transitions has remarkable consequences. First of all, we note that the equations for SHG consist of a number of resonant terms. In this sense the imaginary part, $\text{Im}\chi^{(2)}(-2\omega, \omega, \omega)$ resembles the $\epsilon_2(\omega)$ and provides a link to the band structure.

The difference, however, is that whereas in $\epsilon_2(\omega)$ only the absolute value of the matrix elements squared enters, the matrix elements entering the various terms in $\chi^{(2)}$ are more varied. They are in general complex and can have any sign. Thus, $\text{Im}\chi^{(2)}(-2\omega, \omega, \omega)$ can be both positive and negative. Secondly, there appear both resonances when 2ω equals a interband energy and when ω equals an interband energy. Figures (5-6) shows the 2ω and single ω resonances contributions to $\text{Im}\chi^{(2)}(-2\omega, \omega, \omega)$ compared to $\epsilon_2(\omega)$ (Figures 3-4) for the AgBO_3 . They clearly show a greater variation from high symmetry to lowest symmetry than the linear optic function. In some sense they resemble a modulated spectrum. Third, we note that the 2ω resonances occur at half the frequency corresponding to the interband transition. Thus, the incoming light need not be as high in the UV to detect this higher lying interband transition. This is important for wide band gap materials like many of the ABO_3 compounds where laser light sources reaching the higher interband transitions are not available. Nevertheless, one still needs to be able to detect the corresponding 2ω signal in the UV. Unfortunately the intrinsic richness of $\chi^{(2)}$ spectra remains largely to be explored experimentally we are not aware of any attempts to measure both the real and imaginary parts of these spectral functions as one standard does in linear optics. That is attributed to the fact that the second harmonic response $\chi_{ijk}^{(2)}(\omega)$ contains 2ω resonance along with the usual ω resonance. Both the ω and resonances can be further separated into inter-band and intra-band contributions. The structure in $\chi_{ijk}^{(2)}(\omega)$ can be understood from the structures in $\epsilon_2(\omega)$. Our calculations for $\epsilon_2(\omega)$ give few fundamental oscillators between 1.0 eV and 6.0 eV which correspond to the optical transitions from the valance bands to the conduction band, formed by the d orbitals of the Ta atoms and consisting of two subbands. It is well known that the $\epsilon_2(\omega)$ function computed from moments (\vec{p}) appear to be very sensitive to the ab initio parameters and seem to be particularly appropriate to test electronic band structure. In ABO_3 perovskites the two peak present in experimental reflectivity data are obtained in theoretical curves only when the interband transition moments varied with respect to the energies and \vec{k} wave vectors. In this computation on ABO_3 , compounds many parameters have been barrowed from existing computations have been neglected, explaining some discrepancies between theory and experiments [4-5, 13-19]. The structure 0.5-3.0 eV in $\chi_{ijk}^{(2)}(\omega)$ is associated with interference between ω and 2ω resonances, while the structure above 2.0 eV is due to mainly to ω resonance. In Fig. 5 we show the 2ω interband and intraband contributions for AgBO_3 compounds. Also given is their decomposition into intra- and interband contributions. They are arranged so as to move the $\text{Nb} \rightarrow \text{Ta}$ trends obvious. For example $\chi^{(2)}$ obviously increases when going from Ta to Nb. Unfortunately, the agreement between theory and experiment is by no means perfect [20]. Note that the interband part are negative in all cases and in most cases largely compensate the intraband part. Our compounds in both cases of which interband part is much smaller in magnitude than the intraband part. This quite interesting because unexpected. It raises the question what features in the band structure of these two compounds distinguish them from the other compounds [15,16]. We investigated the reasons for the

cancellation of intra- and interband parts by inspecting the corresponding frequency dependent imaginary parts of the $\chi^{(2)}(-2\omega, \omega, \omega)$. First of all, one now sees that the opposite sign of intra- and interband parts not only occurs in the static value but occurs almost energy by energy.

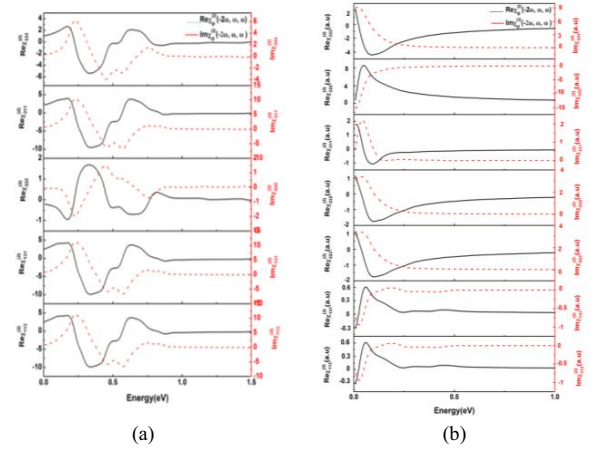


Fig. 5. The calculated total real and imaginary parts of $\chi_{113}^2(\omega)$, $\chi_{131}^2(\omega)$, $\chi_{222}^2(\omega)$, $\chi_{311}^2(\omega)$ and $\chi_{333}^2(\omega)$ for AgTaO_3 (a), and $\chi_{113}^2(\omega)$, $\chi_{131}^2(\omega)$, $\chi_{223}^2(\omega)$, $\chi_{232}^2(\omega)$, $\chi_{311}^2(\omega)$, $\chi_{322}^2(\omega)$, and $\chi_{333}^2(\omega)$ for AgNbO_3 (b).

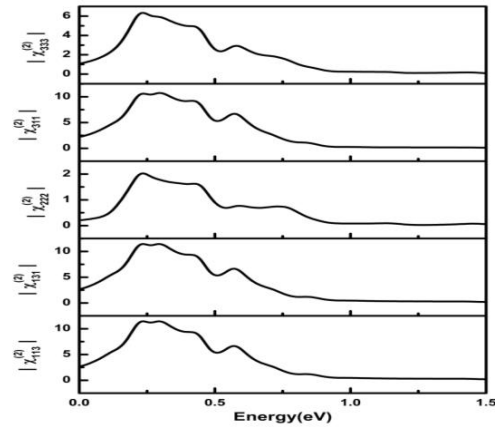


Fig. 6. The calculated total modal parts of $\chi_{113}^2(\omega)$, $\chi_{131}^2(\omega)$, $\chi_{222}^2(\omega)$, $\chi_{311}^2(\omega)$ and $\chi_{333}^2(\omega)$ for AgTaO_3 .

The sign of the inter and intraband part are difficult to understand *a-priori* because a variety of matrix element products comes into play and both ω and 2ω resonances occur in both the pure interband, and the interband contribution modified by intra-band motion when these are further worked out into separate resonance terms. The spectra $\epsilon_2(\omega)$ (Figures 3-4) for the AgBO_3 compounds are rather similar. They look like the superposition of the spectra of more or less four pronounced oscillators with resonance frequencies close to the B and D line structures appearing in the 2ω and ω - terms of the imaginary parts.

As an example of such a prediction the SHG coefficients of AgBO_3 compounds are given in Table 2 and Table 3. For

incident light with a frequency small compared to the energy gap. The independent tensor components are listed for $\omega=0$.

Table 2. Calculated total, intraband and interband of the zero frequency of $\text{Re } \chi_{ijk}^{(2)}(0)$.

Compound	$\text{Re } \chi_{ijk}^{(2)}(0)$	$\chi_{113}^=$	χ_{222}	χ_{311}	χ_{333}	
		χ_{131}				
AgTaO ₃	Total	2.618	-0.208	2.168	1.069	
	Inter1 ω	-0.420	0.053	-0.412	-0.202	
	Inter2 ω	-0.016	-0.022	-0.015	0.028	
	Intra1 ω	-1.095	0.091	-1.115	-0.453	
	Intra2 ω	4.149	-0.331	3.710	1.697	
		$\chi_{113}^=$	$\chi_{223}^=$	χ_{311}	χ_{322}	χ_{333}
		χ_{131}	χ_{232}			
AgNbO ₃	Total	-323.99	1127.46	1775.63	800.32	2160.63
	Inter1 ω	62.86	178.06	213.50	42.86	-324.37
	Inter2 ω	48.09	89.45	-23.78	-8.16	305.45
	Intra1 ω	-122.19	1158.78	1203.26	3612.98	1370.91
	Intra2 ω	-312.75	-298.81	383.65	-2847.3	808.64

Table 3. Calculated total, intraband and interband of the zero frequency of $\text{Im } \chi_{ijk}^{(2)}(0)$.

Compound	$\text{Im } \chi_{ijk}^{(2)}(0)$	$\chi_{113}^=$	χ_{222}	χ_{311}	χ_{333}	
		χ_{131}				
AgTaO ₃	Total	0.859	-0.055	0.724	0.330	
	Inter1 ω	-0.420	0.053	-0.412	-0.202	
	Inter2 ω	-0.016	-0.022	-0.015	0.028	
	Intra1 ω	-1.095	0.091	-1.115	-0.453	
	Intra2 ω	4.149	-0.331	3.710	1.697	
		$\chi_{113}^=$	$\chi_{223}^=$	χ_{311}	χ_{322}	χ_{333}
		χ_{131}	χ_{232}			
AgNbO ₃	Total	-747.92	3058.84	582.01	-	8945.56
	Inter1 ω	229.23	370.35	435.39	-172.51	-449.47
	Inter2 ω	124.10	226.30	-4.08	228.65	154.47
	Intra1 ω	-882.88	706.00	3896.07	7246.51	1739.93
	Intra2 ω	-218.37	1756.18	-3745.3	-	7500.63
						22487.0

IV. CONCLUSION

The linear and nonlinear optical properties of AgBO₃ oxygen-octahedron ferroelectrics have been calculated over a wide energy range. We studied some possible combination of B. This allowed us to study the trends in the second order optical response with chemical composition. The results for the zero-frequency limit of second harmonic generation in agreement with available experimental and theoretical results for other oxygen-octahedron ferroelectrics. The calculated linear electrooptical coefficients for AgTaO₃, is also show agreement with recent experimental data in the energy region below band gap for the other ABO₃ ferroelectrics. For all the considered compounds the SHG coefficient $\chi^{(2)}$ is of the order of $\sim 10^{-7}$ esu. Our calculations of the SHG susceptibility shows that the intra-band and interband contributions are significantly changes with change B and A – ions.

REFERENCES

[1] V. G. Dmitriev, D. N. Gurzadyan and D. N. Nikogosyon, Handbook of Nonlinear Optical Crystals, Berlin, Springer-Verlag, 1991.
[2] H. S. Nalwa (2 nd ed.), Handbook of Advanced Electronic and Photonic Materials and Devices, San Diego: Academic, 2001.
[3] X. Gonze et al, Comp. Mat. Sci. **25**, 478 (2002).
[4] S. Cabuk, H. Akkus and A. M. Mamedov, Physica B **394**, 81 (2007).

[5] S. Cabuk, Optoelectronics and Adv. Mater.-Rapid Commun. **1**, 100 (2007).
[6] R. Cohen and H. Krakauer, "Lattice dynamics and origin of ferroelectricity in BaTiO₃: Linearized-augmented-plane-wave total-energy calculations", Phys. Rev. B vol. 42, pp. 6416-6423, October 1990.
[7] M. Fuch and M. Scheffler, Comput. Phys. Commun. **119**, 67 (1999).
[8] N. Troullier and J. L. Martins, "Efficient pseudopotentials for plane-wave calculations", Phys. Rev. B vol. 43, pp. 1993-2006, January 1990.
[9] J. P. Perdew and Y. Wang, "Accurate and simple analytic representation of the electron-gas correlation energy" Phys. Rev.B vol. 45, pp. 13244-13249, June 1992.
[10] D. M. Ceperley and B. J. Alder, "Ground state of the electron gas by a stochastic method" Phys. Rev. Lett. vol. 45, 566-569, August 1980.
[11] H. J. Monkhorst and J. D. Pack, "Special points for Brillouin-zone integrations", Phys. Rev. B vol.13, pp. 5188-5192, June 1976.
[12] H. Kato, H. Kobayashi, and A. Kudo, "Role of Ag⁺ in the band structures and photocatalytic properties of AgMO₃ (M:Ta and Nb) with the perovskite structure " J. Phys. Chem. B vol. **106**, pp. 12441-12447, November 2002.
[13] A. M. Mamedov and L. S. Gadzhieva, Sov. Phys. States **26** (9), 1732 (1984).
[14] A. M. Mamedov, M. A. Osman and L. C. Hajieva, Appl. Phys. A **34**, 189 (1984).
[15] A. M. Mamedov, Opt. Spektroc. **56** (6), 645 (1984).
[16] M. Veithen, X. Gonze and Ph. Ghosez Ph, "First-principle study of the dielectric and dynamical properties of lithium niobate" Phys. Rev. B vol. 65, pp. 214302-214314, May 2002.
[17] M. Veithen, X. Gonze and Ph. Ghosez, "Nonlinear optical susceptibilities, Raman efficiencies, and electro-optic tensors from first-principles density functional perturbation theory", Phys. Rev. B vol. 71, pp. 125107-125121, March 2005.
[18] X. Y. Meng, Z. Z. Wang, Y. Zhu and C. T. Chen, "Mechanism of the electro-optic effect in the perovskite-type ferroelectric KNbO₃ and LiNbO₃", J.Appl. Phys. vol. **101**, pp. 103506-103512, May 2007.
[19] D. Xue and S. Zhang, Phil. Mag. B **78**, 29 (1998).
[20] D. Xue, K. Betzler and H. Hesse, Optical Materials **16**, 381 (2001).